Pergamon

*Spill Science & Technology Bulletin,* Vol. 6, No. 3/4, pp. 225–237, 2000

Printed in Great Britain
1353-2561/01 $ - see front matter

PII: S1353-2561(01)00041-X

RESEARCH

# Vertical Mixing by Langmuir Circulations

JAMES C. McWILLIAMS†* & PETER P. SULLIVAN‡
†*University of California at Los Angeles, Los Angeles, CA 90095-1565, USA*
‡*NCAR, Boulder, CO 80307-3000, USA*

**Wind and surface wave frequently induce Langmuir circulations (LC) in the upper ocean, and the LC contribute to mixing materials down from the surface. In this paper we analyze large-eddy simulation (LES) cases based on surface-wave-averaged, dynamical equations and show that the effect of the LC is a great increase in the vertical mixing efficiency for both material properties and momentum. We provide new confirmation that the previously proposed K-profile parameterization (KPP) model accurately characterizes the turbulent transport in a weakly convective, wind-driven boundary layer with stable interior stratification. We also propose a modest generalization of KPP for the regime of weakly convective Langmuir turbulence. This makes the KPP turbulent flux profiles match those in the LES case with LC present fairly well, especially so for material properties being transported downwards from the ocean surface. However, some open issues remain about how well the present LES and KPP formulations represent Langmuir turbulence, in part because wave-breaking effects are not yet included.** © **2001 Elsevier Science Ltd. All rights reserved.**

## Introduction

If polluting material spilled into the ocean does not rapidly evaporate or sink, it is moved and mixed over many days mainly under the influences of surface-gravity waves and near-surface currents. The influential types of currents in coastal regions are tides, geostrophic flows (with the Coriolis force balancing the pressure force from sea level slopes unrelated to surface waves) and both mean and turbulent motions in the surface planetary boundary layer. The boundary layer occurs because surface wind stress and heat and water fluxes induce nearby shear and stratification instabilities that lead to vigorous, turbulent fluctuations. The boundary layer has a thickness typically on the order of tens of meters, though occasionally it is much thinner or thicker when surface heating or cooling is extreme. Its depth of penetration into the oceanic interior usually is limited by a stable density stratification underneath (the pycnocline).

*Corresponding author.

Mariners frequently see wind rows, which are streaks of surfactants usually aligned with the wind and/or waves. The spacing between streaks is highly variable, of course, but it typically is some meters or tens of meters and thus comparable to both the wavelength of surface-gravity waves and the boundary-layer depth. The oceanographic interpretation of wind rows is that they result from lines of convergence in the surface currents associated with Langmuir circulations (LC) (Leibovich, 1983). The LC are believed to occur quite commonly, even more so than is evident under favorable surfactant viewing conditions. The dynamical origin of the LC is understood as a wind-driven shear instability in combination with surface wave influences related to their mean Lagrangian motion, called Stokes drift (Craik & Leibovich, 1976).

How do the LC contribute to the movement and dispersal of spilled materials? Because the LC are local recirculations over tens of meters, they contribute little to the systematic displacement (i.e., advection) of materials compared to the contributions of tides, geostrophic flows, and mean boundary-layer currents (though they do partly control the shape of latter; see Section 2). They do, however, contribute to the spreading, hence dilution, of the material.

The spreading rate by turbulent currents is commonly expressed in terms of an eddy diffusivity, $\kappa$, where the expected size of a spill is $D \sim \sqrt{\kappa T}$ after some time $T$ that encompasses many cycles of the turbulent eddies. It is also common to make a rough estimate for a diffusivity by $\kappa \sim VL$, where $V$ is a characteristic eddy velocity and $L$ an eddy correlation length for fluctuating currents that cause the spreading. For horizontal spreading by the LC, therefore, we can use $V \approx 0.1$ m/s and $L \approx 10$ m to estimate $\kappa_h \sim 1$ m$^2$/s (with subscript h for horizontal), hence $D_h \sim 300$ m after $T \approx 1$ day. [1] This is not a large distance. In contrast, mesoscale geostrophic eddies typically have horizontal $V$ values at least as large as the LC and horizontal $L$ values much larger $t \sim 10$ s km. Thus, we expect their $\kappa_h$ values to be much larger than those for the LC and accordingly their influences to be more important for horizontal dispersal of material.

The situation is quite different for spreading material in the vertical. Tides, geostrophic flows, and mean boundary-layer currents are primarily horizontal in their motions, hence inefficient in vertical dispersal. Surface waves do have strong vertical motions, and breaking waves in particular contribute significantly to moving materials from the surface into the oceanic interior, though usually over a depth of only a few meters. The primary mechanism for vertical dispersal is by boundary-layer turbulence, and, as shown below, the LC are an especially efficient type of boundary-layer motion in causing vertical mixing. The same $V$, $L$, and $\kappa$ estimates as above are relevant to vertical motions in LC, hence we estimate $\kappa_v \sim \kappa_h \sim 1$ m$^2$/s, which is not small compared to contributions from other types of currents and which can fill the whole of the surface boundary layer with mixed material in a fraction of a day.

In this paper, we present a model that may be useful for estimating the vertical spreading of material in the upper ocean under conditions in which LC occur. Its basis is computational simulations of turbulent boundary layer currents with LC (Section 2). In the framework of a widely used turbulent mixing model (Section 3), we propose generalizations that include LC effects (Section 4). Finally, we suggest how this mixing model could be further developed and implemented for practical applications to tracking and predicting the movement of materials spilled into the ocean (Section 5).

[1] This estimate is most relevant to transverse dispersal, i.e., in the direction perpendicular to the wind rows. Since longitudinal correlation lengths are greater for LC, longitudinal dispersal will be somewhat more efficient.

## Langmuir Turbulence

Measurements in the oceanic boundary layer are notoriously difficult to make, for many reasons, and our approach here is to rely mainly on computational simulations of boundary layer turbulence to provide information about vertical transport and mixing by the LC. Computational simulations are widely used in oceanography now, with considerable confidence in the qualitative behavior evinced when the calculation is physically well conceived and the influences of unresolved (i.e., sub-grid scale, [SGS]) motions are not delicate. The greatest limitation with this approach is the difficulty achieving an overview of parametric and computational sensitivities. At present we have only a few relevant simulation cases available, and consequently our proposed mixing model in Section 4 is less comprehensive than ultimately needed for general usage.

The simulation is done by computational time integration of the following equations discretized on a 3D spatial grid:

$$\begin{aligned}
&\frac{\mathrm{D}\mathbf{u}}{\mathrm{D}t} + 2\Omega \times \mathbf{u} + \frac{1}{\rho_0}\nabla P + \hat{\mathbf{z}}\frac{g\rho}{\rho_0} + \mathrm{SGS} = \mathbf{u}^s \times (2\Omega + \nabla \times \mathbf{u}),\\
&\frac{\mathrm{D}c}{\mathrm{D}t} + \mathrm{SGS} = -\mathbf{u}^s \cdot \nabla c,\\
&\nabla \cdot \mathbf{u} = 0, \qquad (1)
\end{aligned}$$

where $\mathbf{u}$ is the velocity; $P$ is the pressure; $\rho$ is the density; and $\rho_0$ is an average value; $c$ is any materially conserved scalar quantity (e.g., temperature $T$, salinity $S$, or a chemical concentration); $\Omega$ is the Earth's rotation vector; $g$ is the gravitational acceleration; $\hat{\mathbf{z}}$ is a unit vertical vector, aligned anti-parallel to gravity; and the operator

$$\frac{\mathrm{D}}{\mathrm{D}t} = \frac{\partial}{\partial t} + \mathbf{u} \cdot \nabla$$

is the advective time derivative. SGS denotes non-conservative terms due to any internal sources and sinks (including chemical reactions) and the effects of unresolved scales of motion and molecular diffusion; in the simulation approach we use, called large-eddy simulation (LES), the SGS prescriptions are based on single-point, second-moment turbulence closure models (McWilliams *et al.*, 1999, for a summary). The terms on the right-hand sides in (1) represent averaged dynamical effects of surface gravity waves on the more slowly evolving currents calculated with (1) (Craik & Leibovich, 1976; McWilliams & Restrepo, 1999); these terms involve the waves' Stokes drift,

$$\mathbf{u}^s(z) = \overline{\left( \int^t \mathbf{u}^w(\mathbf{x}, s)\, \mathrm{d}s \cdot \nabla \right) \mathbf{u}^w},$$

where $\mathbf{u}^w$ is the wave orbital velocity and the overbar denotes an average over the waves. The system (1) is closed by the oceanic equation of state, $\rho[P, T, S]$, and appropriate boundary conditions, including surface fluxes of momentum and scalar quantities.

It is widely believed that the wave-averaged vortex force, represented in (1) by the final term in the momentum equation, is an essential element of the dynamics of LC. To date only a few boundary-layer LES cases have been calculated with the vortex force included (Skyllingstad & Denbo, 1995; McWilliams *et al.*, 1997; Skyllingstad *et al.*, 1999, 2000; Skyllingstad, 2000); these we call Langmuir turbulence, since the flows are manifestly turbulent and the LC are evident in flow visualizations. Figure 1 is a sketch of the posing of such a calculation for a stratified Ekman layer with waves. Specifically, we calculate a LES case [2] for a mid-latitude, deep-water region with a uniform wind stress, $\tau = \rho_0 u_*^2 = 0.037\ \mathrm{N/m^2}$ ($u_* = 0.0061$ m/s) in the $+x$ direction at the ocean surface, $z = 0$, as well as a monochromatic surface gravity wave field propagating in the same direction with an elevation amplitude of 0.8 m and wavelength of $\lambda = 60$ m, hence $u^s(z) = U^s \exp[4\pi z/\lambda]$ with $U^s = 0.068$ m/s. The initial $\rho$ and $T$ fields are fairly well mixed near the surface over a depth of $h = 35$ m, with a stable stratification underneath with stability frequency $N = 0.0044\ l$/s. In addition there is a weak, uniform cooling of the surface at 5 $\mathrm{W/m^2}$. After an adjustment period of several hours, the flow reaches a quasi-equilibrium, turbulent state, with a weak evolutionary deepening of the layer due to entrainment fluxes near $z = -h$. An eddy turn-over time $T_e = h/u_*$, is about 6100 s here, the statistical averaging time during the quasi-equilibrium phase is more than $10T_e$, and the average boundary-layer thickness during this phase is $h \approx 37.5$ m.

In this case the relative influences of winds and waves are characteristic of equilibrium wind waves (except for the simplifications of no wind fluctuations and a wave spectrum with only a singly dominant component); quantitatively, this is expressed by the non-dimensional Langmuir number,

$$La = \sqrt{\frac{u_*}{U^s}}\,, \tag{2}$$

having a typical value, here 0.3.

The presence of LC in this LES case is demonstrated by their effects on organizing a field of surfactant (Fig. 2), which is released randomly throughout the model domain at a time during the quasi-equilibrium period. Each surfactant parcel moves horizontally on the surface according to the equation,

$$\frac{\mathrm{d}\mathbf{x}_h}{\mathrm{d}t} = \mathbf{u}_h(\mathbf{x}_h, 0, t) + \mathbf{u}_h^s(0),$$

where the subscript h denotes the horizontal component of a vector. The Eulerian surface velocity $\mathbf{u}_h$ is taken from the LES, and $\mathbf{u}^s$ is added so that the parcel moves with the wave-averaged Lagrangian velocity. Within minutes almost all the surfactant moves into somewhat irregular, but wind/wave-aligned convergence lines associated with the LC, as well as being displaced *en masse* by the mean Lagrangian flow (here towards the south-east). In many places the convergence lines intersect in Y-junctions with the stem line pointed down-wind/wave, as observed. On a time scale longer than it takes for the parcels to collect in the convergence lines, the point of intersection often moves like a zipper to merge two adjacent LC cells; this opens up space for a new convergence line to develop nearby, thus maintaining an equilibrium cycle of LC generation and disappearance. In an otherwise identical LES case without the wave-averaged terms in (1) (i.e., with $La = \infty$), there is very much less trapping of the surfactant into lines, [3] indicating that the LC are especially efficient material collectors. In different LES cases with different values of $La \leqslant \mathcal{O}(1)$ and $h/\lambda$, we see differing degrees of regularity in the surface convergence-line patterns.

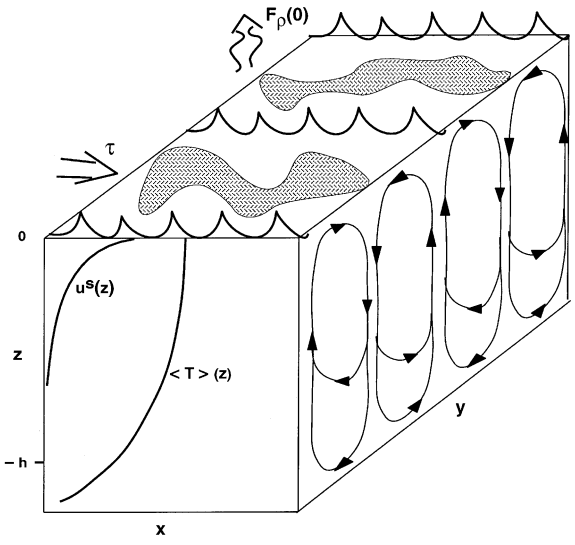


**Fig. 1** Sketch of the oceanic surface boundary layer with LC present.

[2] This LES case is more extensively but differently analyzed in McWilliams *et al.* (1997).

[3] See McWilliams *et al.* (1997) for several visualizations of the pattern differences between $La = 0$ and $\infty$.

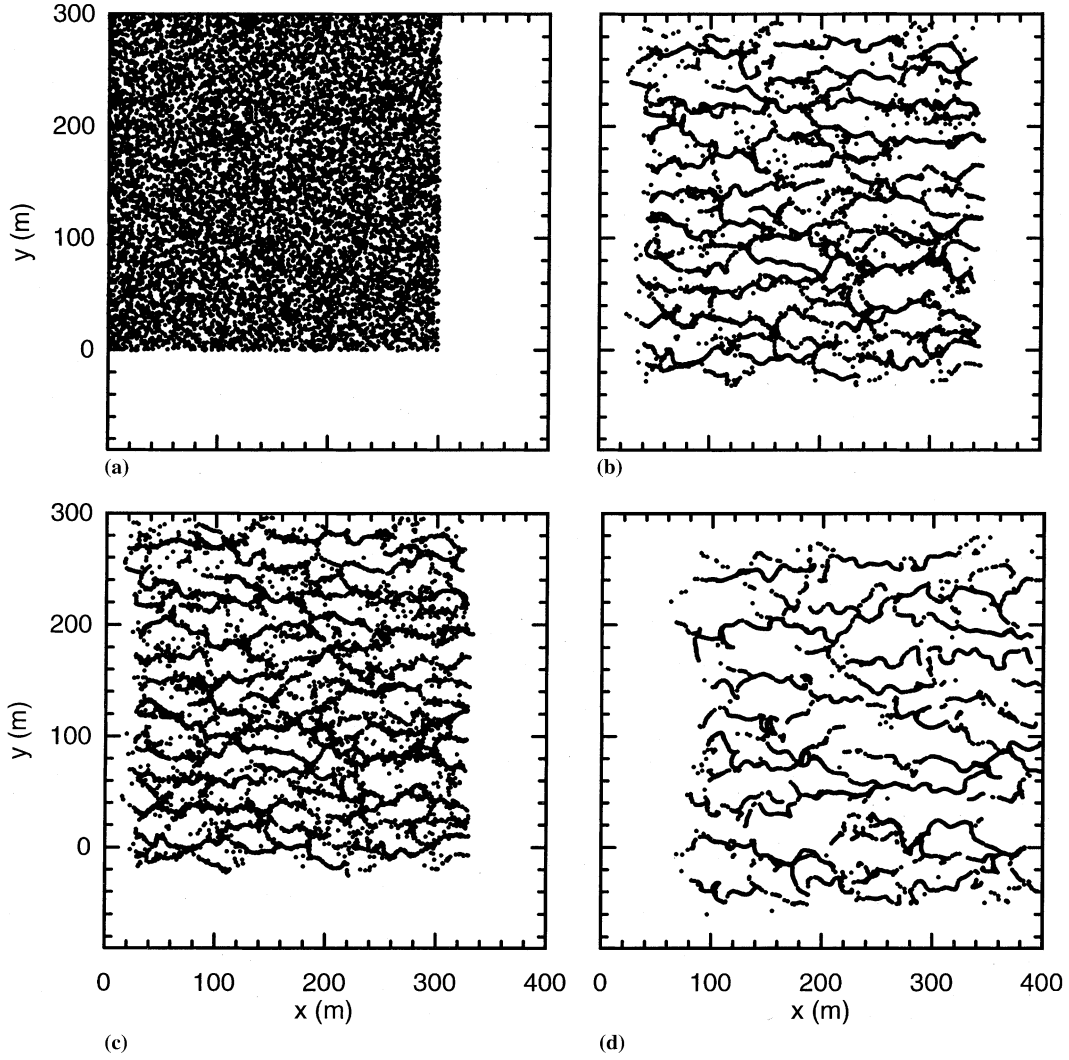


**Fig. 2** Surface particles at several times after being released randomly at $t = 0$ for the LES case with $La = 0.3$. Panels (a)–(d) are for $t = 0, 440, 672$, and 1480 s, respectively.

The turbulent flow statistics are markedly different in Langmuir turbulence than in an Ekman layer without wave influences. This is illustrated by comparing the turbulent kinetic energy and dissipation-rate profiles between LES cases with $La = 0.3$ and $\infty$ (Fig. 3): Langmuir turbulence is much more energetic and has a stronger energy cycle (i.e., eddy generation by instability and dissipation by cascade to small scales). The LC comprise part of the enhanced variability in Langmuir turbulence but so also do other less obviously coherent patterns of fluctuating currents. In addition, the mean current profiles, $\langle \mathbf{u}_h \rangle(z)$, are substantially different in Langmuir turbulence, both by exhibiting less vertical shear within the boundary layer and by turning further from the wind in an anticyclonic direction than do classical Ekman currents. The turbulent mixing rates are also faster in Langmuir turbulence, as might be expected from the greater turbulent energy. These will be analyzed in Section 4, after a diagnostic framework is established in Section 3.

## K-Profile Parameterization

Computational simulation is a powerful methodology, but it is inherently incapable of spanning the full range of oceanic currents (hence, e.g., the need for SGS schemes in boundary-layer LES). It also is too cumbersome for frequent scientific uses and practical applications that require a rapid response (such as pollution spills). Therefore, a less fundamental but much simpler model of the boundary layer, in which the effects of the turbulence are parameterized rather than calculated from fluid dynamics, is desirable. It is thus reasonable to have somewhat limited expecta-

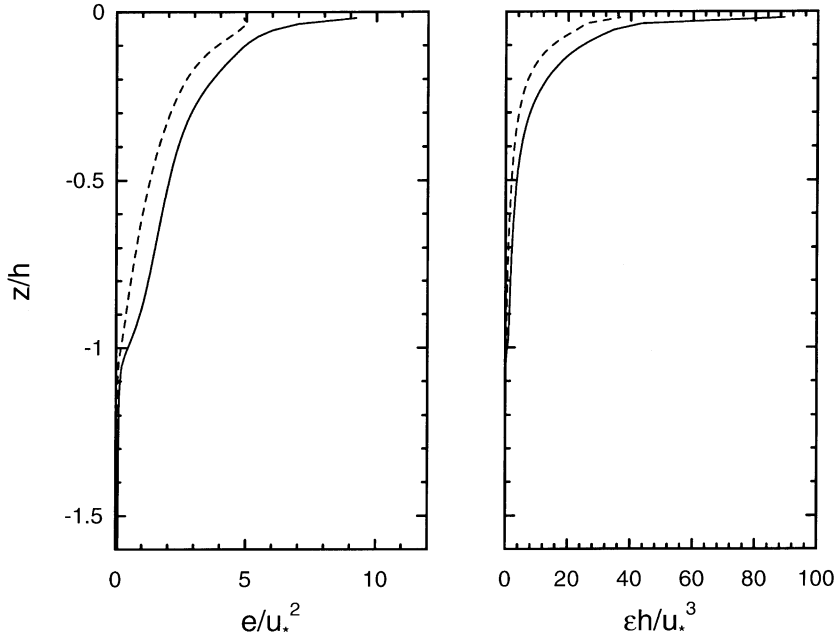


**Fig. 3** Turbulent kinetic energy, $e(z) = \frac{1}{2}\langle \mathbf{u}'^2 \rangle$, and dissipation rate, $\epsilon(z)$, for LES cases with and without LC effects (i.e., $La = 0.3$ [solid] and $\infty$ [dashed]). Normalizations are by $u_*^2$ and $u_*^3/h$, respectively, and the depth is normalized by $h$.

tions for a useful parameterization: it must represent the hypothesized essential effects with qualitative validity; it must be fit and assessed quantitatively in at least some situations; and it must not lead to silly answers in general applications, even though it might not always be particularly accurate.

The K-profile parameterization (KPP) is a model of vertical transport and mixing within the planetary boundary layer that has been found to meet the criteria above fairly well. In KPP the evolution of a fluid quantity $Q$ (i.e., horizontal velocity or a material tracer) is influenced by transport and mixing according to an equation of the following form:

$$\frac{\partial \langle Q \rangle}{\partial t} = \cdots + \frac{\partial F_Q}{\partial z}, \tag{3}$$

where the angle brackets denote an average in time and horizontal position over the scales of surface waves and boundary-layer turbulence, $F_Q$ is the mean vertical flux of $Q$ by the waves, turbulence, and molecular diffusion,

$$F_Q(z) \equiv -\langle Q'w' \rangle + \kappa_m \frac{\partial \langle Q \rangle}{\partial z} \tag{4}$$

($\kappa_m$ is the molecular diffusivity), and the dots in (3) denote other evolutionary influences unrelated to the waves and turbulence, including any non-conservative, material processes or even buoyancy forces (such as air bubbles and oil droplets). In the KPP model the flux within the boundary layer, $0 \geqslant z \geqslant -h$, has the following form:

$$F_Q(z) = \kappa_{v,Q}(z)\left[\frac{\partial \langle Q \rangle}{\partial z} - \gamma_Q\right], \tag{5}$$

where $\kappa_{v,Q}$ is a positive eddy diffusivity profile; $\gamma$ appears here as an augmentation of the mean $Q$ gradient; and $-\kappa\gamma$ is a flux profile independent of the mean gradient (often called the counter-gradient flux).

O'Brien (1970) noted that $\kappa_v$ usually has a convex structure in the boundary layer. With this assumption as its basis, KPP was formulated and tested empirically as an atmospheric model in Troen and Mahrt (1986) and as an oceanic model in Large *et al.* (1995). It was evaluated by comparison with computational boundary-layer simulations in Ayotte *et al.* (1996), and its performance is assessed in oceanic general-circulation models in Large *et al.* (1997), Large and Gent (1999), and Li *et al.* (2000). The experience with it has been generally judged satisfactory in the various contexts where it has been used, which spans a wide range of conditions in surface stress and buoyancy flux, as well as interior stratification and currents. As yet it has not been assessed by observations or LES cases where LC are active, nor do its present rules include any dependence on *La* (remedied in Section 4).

KPP is a non-local, mean-field closure model, since $\kappa$ and $\gamma$ are functionals of the surface boundary fluxes and mean quantities throughout the whole boundary layer. Thus, it is quite different from other commonly used boundary-layer models, such as a mixed-layer model (where the mean profiles are specified rather than the fluxes), a single-point, second or third moment closure model (which is wholly local), or a

surface-layer (i.e., Monin–Obukhov, M–O) similarity model (based entirely on the surface fluxes). Each of these qualitative differences allows KPP to have potentially greater oceanic realism than any of the alternatives.

Now we describe the current rules for the KPP scheme, in a simpler way by ignoring the niceties of absorbed solar radiation and the boundary-layer structure very near the top surface, [4] and the special case of no interior pycnocline; a complete description is in Large *et al.* (1995).

The boundary-layer depth, $h$, is determined in KPP as the smallest $h$ for which a boundary-layer Richardson number,

$$Ri_{\mathrm{b}} = \frac{gh \mid \Delta[\langle\rho\rangle] \mid}{\rho_0(\mid \Delta[\langle\mathbf{u}\rangle] \mid^2 + W^2)} \tag{6}$$

rises above a specified critical value, as it always will when a significant pycnocline is present. Here the operator $\Delta$ denotes the difference in values between $z = 0$ and $-h$, and $W$ is a turbulent velocity magnitude (defined in (9) or (11) below).

The eddy diffusivity, $\kappa(z)$, is assumed to have a self-similar, convex shape across the boundary layer and an amplitude related to the fluxes at the edges of the layer. Its formula is

$$\kappa_{\mathrm{v}} = WhG(\sigma), \tag{7}$$

where $\sigma = -(z/h)$ is the normalized depth within the layer. $G(\sigma)$ is the shape function. In the canonical situation with M–O similarity structure near $z = 0$ and negligible mixing below $z = -h$, then

$$G = \sigma(1-\sigma)^2, \tag{8}$$

which vanishes at the top and bottom of the boundary layer (i.e., $\sigma = 0$ and 1, respectively) and has a maximum value of 0.15 at $\sigma = 0.33$. $W$ is a turbulent velocity scale,

$$W = \frac{ku_*}{\phi}, \tag{9}$$

where $k = 0.4$ is Von Karman's constant and $\phi$ is the well-known stability function in M–O theory. In the KPP model, $\phi$ is a function of $h/Z$ outside of the near-surface layer (i.e., $0 \geqslant -z \geqslant 0.1h$), and its values differ between scalar quantities and momentum when $Z < 0$. Here

$$Z = -\frac{\rho_0 u_*^3}{gkF_\rho(0)}$$

is the M–O length.

The non-gradient flux, $\gamma(z)$, is assumed in KPP to have a uniform profile throughout the interior part of the boundary layer,

$$\gamma = -\mathscr{C}_\gamma^* \frac{F_Q(0)}{Wh}, \tag{10}$$

where $\mathscr{C}_\gamma^*$ is a positive constant. This formula implies that – after the multiplication by the positive, convex $\kappa(z)$ in (5) – there is a transport of $Q$ from the upper part of the boundary layer (i.e., above the maximum in $G$) to the lower part (below the maximum) in the sense set by the sign of the surface flux, $F_Q(0)$. [5] This is an intrinsically non-local flux process, since it is not linked to the local mean gradient at any particular depth. The utility of $\gamma$ was recognized by Deardorff (1972) for convective boundary layers in which gravitationally unstable plumes carry heat and material across the boundary layer, even though the interior mean gradients are small; of course, an analogous statement can be made for the LC, some of which also span the whole boundary layer. For temperature in thermal convection, the mean gradient even reverses sign within the layer due to entrainment of interior fluid that provides a heat flux near the edge of the layer with a sign opposite to the surface flux, but the sign reversals of $F_Q$ and $\partial\langle Q\rangle/\partial z$ rarely occur at the same $z$ value. Thus, $\gamma$ can prevent singularities and negative values in $\kappa(z)$ when (5) is fit to actual profiles of $F_Q(z)$ and $\langle Q\rangle(z)$, and $\gamma$ is commonly fit simultaneously to make $\kappa(z) > 0$ and smooth in $z$. [6] In the present KPP scheme, $\gamma$ is taken to be non-zero, from (10), only for scalar $Q$ quantities (i.e., not for $\mathbf{u}_{\mathrm{h}}$) and only in the convective regime where $F_\rho(0) > 0$. The rationale for this restriction is a minimalist one, not to invoke a process except where it has been shown to be needed. However, it is probably useful for any quantity with opposing surface and entrainment fluxes on small mean gradients, by the argument above, and it probably does little or no harm otherwise since mean

[4] In its present formulation, the KPP rules yield both fluxes and mean profiles consistent with similarity theory near the boundary. We do not focus on the surface region in this paper. In part this is to make our preliminary proposal for including LC effects in KPP simpler. More importantly, though, it is because wave breaking is known to cause significant deviations from M–O similarity structure near the surface (Terray *et al.*, 1996), so that a further revison of KPP is needed for this behavior anyway, which we are not yet prepared to make.

[5] For example, surface cooling implies $F_T(0) < 0$, hence $\gamma > 0$, hence $-\kappa\gamma < 0$ and its divergence acts in (3) to increase $T$ in the upper part of the boundary layer and cool the lower part and thus contributes to the movement of heat from below up towards the surface.

[6] Without $\gamma$, an eddy-diffusion model like (3)–(5), with a smooth, positive $\kappa$, will make $\langle Q\rangle(z,t)$ evolve such that zeros in $F_Q$ and the mean gradient occur in the same location, unlike what is observed in convective boundary layers, for example.

gradients tend not to be so small when these edge fluxes are not in opposition; this issue is further discussed in the next section.

## Mixing Effects by Langmuir Circulations

We now analyze the LES solutions with and without LC (Section 2) and fit their calculated mixing rates with a generalization of the KPP model (Section 3). The basis for the generalization is experimental evidence that, when LC are evident, the near-surface, transverse velocity amplitude (i.e., the horizontal component perpendicular to wind and wave directions) varies in direct proportion to $U^s$; this has been found both in observations (Smith, 1998, 1999) [7] and in Langmuir turbulence LES (Skyllingstad, 2000), although the empirical data base is still modest and there is still uncertainty about what the value of the proportionality coefficient is (or may otherwise depend on). Nevertheless, this empirical proportionality suggests a simple modification of KPP so that the turbulent velocity scale relevant to the mixing rates, $W$ in (7), (9), and (10), also has this behavior. [8]

An alternative definition with this property is

$$W = \frac{ku_*}{\phi} \cdot \mathscr{E}, \quad \mathscr{E} = \left[1 + \frac{\mathscr{C}_W}{La^{2\alpha}}\right]^{1/\alpha}, \tag{11}$$

where $\mathscr{E} \geqslant 1$ is an enhancement factor due to the presence of LC (i.e., $\mathscr{E}$ increases as $La$ decreases), with $\mathscr{C}_W$ and $\alpha$ positive constants. The choice of $\alpha$ is not well constrained by present evidence, so we somewhat arbitrarily choose $\alpha = 2$, essentially for reasons of mathematical esthetics (this is analogous to the common use of a least-squares error norm for data analysis). In any event $\alpha$ only governs the shape of $W(La)$ in the narrow transition regime between shear and Langmuir regimes. Given the choice in (11), we determine $\mathscr{C}_\gamma$ and $\mathscr{C}_W$ by fitting $\kappa$ and $\gamma$ to our LES cases. The relation (11) recovers the previous KPP relation (9) when wave effects are weak (i.e., $La$ is large). It also implies that $W \propto U^s$ when $La$ is small, as intended.

The LES cases in Section 2 have a $Z$ value of $-240$ m, indicating that these are simulations of weakly convective, wind-driven, shear boundary layer. Accordingly, $h/Z = -0.14$ is small, and the value of the stability function, $\phi = 0.95$ for momentum and 0.90 for scalar quantities, as calculated from eqn (B1) of Large *et al.* (1995). Thus, these cases do not allow us to test whether there are important stability dependences in (11), e.g., in the coefficient $\mathscr{C}_W$. For now there remains an unsettled physical issue about how the LC behave and affect the turbulent mixing rates in the boundary layer when the surface density flux is either strongly stabilizing ($\phi \gg 1$) or convective ($\phi \ll 1$). Similarly, from our own exploratory LES cases and form Skyllingstad (2000), we know that there are sensitivities to the value of $h/\lambda$, especially when this ratio becomes very small (smaller than in the present cases with $h/\lambda \approx 0.6$). For all these reasons, we must view the present proposal for generalizing KPP as provisional, pending a much broader survey of regimes in surface buoyancy flux and stratification.

We start the assessment of this proposal with the density field, which has been the primary basis for choosing the KPP form (5). In Fig. 4 are shown the mean density profile, the turbulent density flux, and the associated vertical diffusivity $\kappa_{\mathrm{v},\rho}$. Note that the density profile shows a larger change from its initial shape with LC present, due to the substantially increased entrainment flux and enhanced diffusivity throughout the boundary layer. The diffusivity is calculated from (5), after fitting the value of $\gamma$ to maximize the smoothness in $\kappa(z)$ in the vicinity of $\partial\langle\rho\rangle/\partial z = 0$. We represent the non-gradient flux by

$$\gamma = -\mathscr{C}_\gamma \frac{F_Q(0)}{Wh}, \tag{12}$$

which is identical to (10) but here with a distinct coefficient, $\mathscr{C}_\gamma$. The fitted value $\mathscr{C}_\gamma \approx 1.04$ yields smooth $\kappa$ profiles for both LES cases, with and without LC, [9] and the sensititvity of the $\mathscr{C}_\gamma$ fit is illustrated in Fig. 5. The corresponding ratio of peak values for $\kappa$ has a ratio of approximately 3.25 as shown in Fig. 4(c); from (7) and (11), this ratio is equal to the ratio of the turbulent velocity scales, $W$, with an enhancement factor due to the LC of $\mathscr{E} \approx 3.25$, whence $\mathscr{C}_W = 0.080$. Furthermore, the shape of $\kappa(z)$ is close to the convex KPP form of $G(\sigma)$ in (8), and the peak magnitude of $\kappa/u_*h$ is very close to the value of

[7] In Plueddemann *et al.* (1996) a different empirical dependence on $U^s$ was proposed, based in part on prior theoretical arguments, but these data also shown by Smith (1998) to be consistent with linear proportionality.

[8] It is, of course, implausible that this linear relationship for $W$ would continue all the way to $La \to 0$, which would imply an efficient turbulent mixing of mean gradients even when the surface stress vanishes. However, the empirical evidence supporting this relationship and the present LES cases are nowhere near this limit, so for now we will not attempt to regularize it.

[9] This value is smaller than that proposed in Large *et al.* (1995), following earlier precedents; there, for (10), the value of $\mathscr{C}^*_\gamma \approx 6$ was chosen to match the regime of free convection, $h/Z \to -\infty$ (e.g., Holtslag & Moeng, 1991), rather than the much smaller value of our LES cases here, $h/Z = -0.14$. Taken together with the present results, we conclude that $\mathscr{C}^*_\gamma$ and $\mathscr{C}_\gamma$ should have a monotonically increasing dependence on $-h/Z \geqslant 0$ (as does $\phi$ in M–O theory), and possibly on $La$ as well, but we do not yet have a sufficient data base to determine this dependence in a formulaic way.

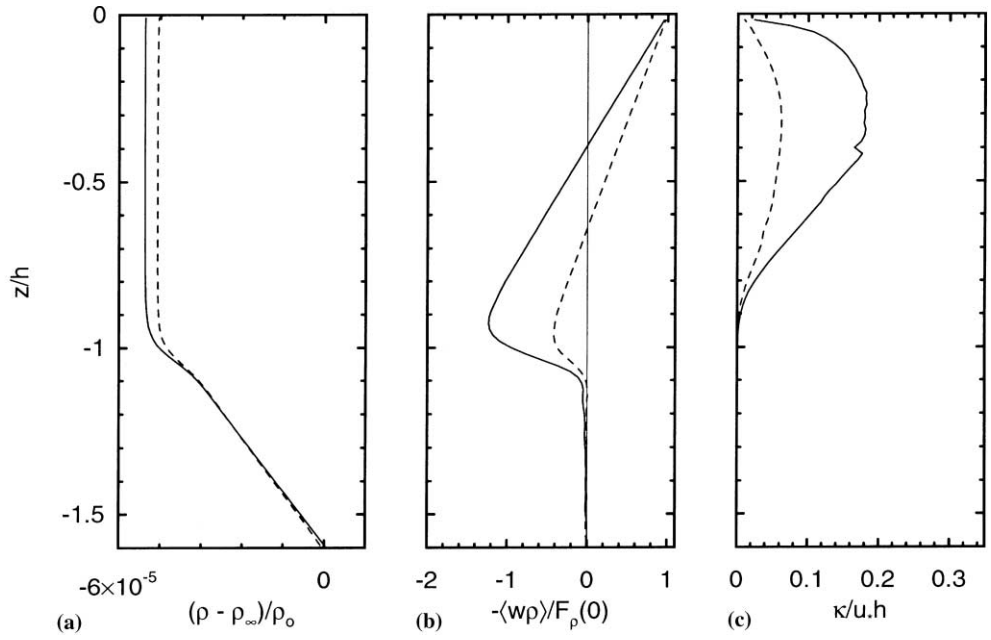


**Fig. 4** Vertical profiles related to density for LES cases with and without LC effects (i.e., $La = 0.3$ [solid] and $\infty$ [dashed]): (a) mean, $\langle\rho\rangle(z) - \langle\rho\rangle(-60\text{ m})$ (normalized by $\rho_0$); (b) turbulent flux, $\langle\rho' w'\rangle(z)$ (normalized by $-F_\rho(0)$); and (c) eddy diffusivity, $\kappa_{v,p}(z)$ (normalized by $u_* h$). The value $\mathscr{C}_\gamma = 1.04$ is used here.

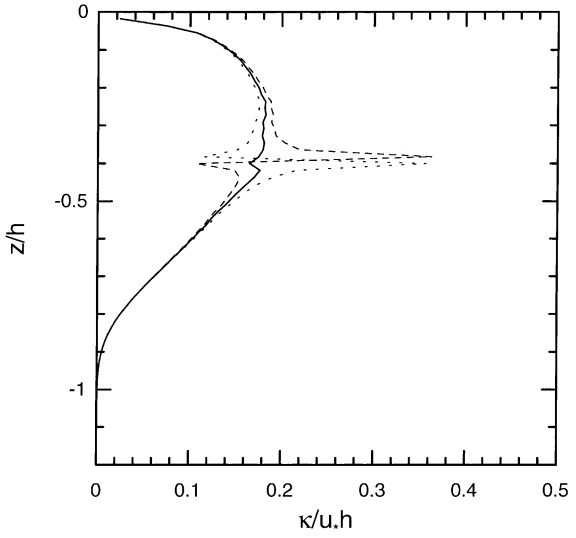


**Fig. 5** Fitting the eddy diffusivity for density, $\kappa_{v,p}(z)$ from (4) and (5), with different choices of $\mathscr{C}_\gamma$ for the LES case with $La = 0.3$: $\mathscr{C}_\gamma = 0.93$ [dashed], 1.04 [solid], and 1.14 [dotted].

$k\mathscr{E}/\phi \cdot \max[G] \approx 0.067\mathscr{E}$ in (7). [10] The peak values of $\kappa$ in Fig. 4(c) also match well what is diagnosed in free convection, given the appropriate change in the turbulent velocity scale with $\phi[h/Z]$ (see Holtslag & Moeng, 1991, Fig. 5). Thus, the generalized KPP form represents the density mixing profile rather well, simply by an enhancement of $W$ with an increasing dependence on $La$ and appropriate choices of the constants $\mathscr{C}_\gamma$ and $\mathscr{C}_W$.

We can assess material mixing more generally by including passive tracers in the LES calculation. Following Wyngaard and Brost (1984), Wyngaard (1987), and Wyngaard and Weil (1991), a useful distinction has been made in convection between tracers being mixed from the interior by an entrainment flux into the boundary layer (i.e., 'to-boundary' scalars, which we denote by the subscript $\rightarrow 0$) and tracers being mixed away from the surface and out of the boundary layer due to injection by a surface flux (i.e., 'from-boundary' scalars which we denote by the subscript $0 \rightarrow$). [11] Density is a particular combination of to- and from-boundary scalars, with the former dominating in the present, weakly convective LC cases (Fig. 4(b)) and the latter dominating in free convection. The reason for this distinction is that $\kappa_{v,\rightarrow 0} > \kappa_{v,0\rightarrow}$ in free convection, by about a factor of 2; this is interpreted as an effect of coherent plumes and the associated from-boundary skewness of the vertical velocity field, $w$. Since the LC also provide a coherent transport across the whole boundary layer and also exhibit a significant from-

[10] Notice that the magnitude of $\kappa_v$ is smaller than estimated in Section 1 because the correlation coefficient between the quantities that comprise the turbulent flux is much less than one. However, the enhancement of $\kappa$ by LC is greater on average than the enhancements of $e$ and $\epsilon$ in Fig. 3, indicating that the LC are atypically efficient turbulent motions in producing a mean flux.

[11] Our nomenclature differs from the 'top-down' and 'bottom-up' names in usage for the atmospheric boundary layer in order to able to be discuss both the atmospheric and oceanic cases in a common way.

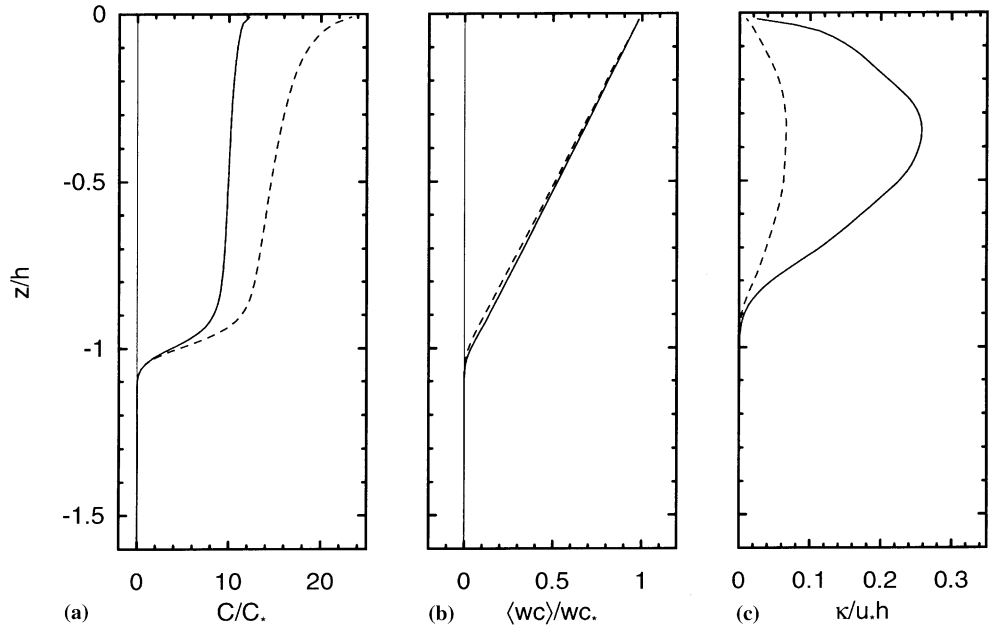


**Fig. 6** Vertical profiles related to the from-boundary scalar concentration, $c_{0\rightarrow}$, for LES cases with and without LC effects (i.e., $La = 0.3$ [solid] and $\infty$ [dashed]): (a) mean, $\langle c_{0\rightarrow}\rangle(z)$ (normalized by $c_* = F_{0\rightarrow}(0)/u_*$); (b) turbulent flux, $\langle c'_{0\rightarrow}w'\rangle(z)$ (normalized by $-F_{0\rightarrow}(0)$); and (c) eddy diffusivity, $\kappa_{v,0\rightarrow}(z)$ (normalized by $u_*h$). The value $\mathscr{C}_\gamma = 1.04$ is used here.

boundary (i.e., downwelling) skewness in $w$, we believe the distinction may also be relevant for the regime of Langmuir turbulence. The present KPP rules (Section 3) do not make a distinction between different scalars, hence they do not yield different $\kappa(z)$ profiles for to- and from-boundary scalars.

A from-boundary scalar field, $c_{0\rightarrow}$, has a surface flux into the ocean with initially zero values everywhere. With time its interior concentration increases, more so in the boundary layer and less so in the interior due to small mixing across the edge of the entraining boundary layer. Fig. 6 shows the mean, turbulent-flux, and eddy-diffusivity profiles for $c_{0\rightarrow}$ during the slowly evolving, quasi-equilibrium phase. The diffusivity is fit exactly as for density, using the same value for $\mathscr{C}_\gamma$, as required by the present KPP rules (Section 3). The flux profiles are essentially linear in $\sigma = -z/h$, from the specified surface flux to the necessarily zero entrainment flux (since $c_{0\rightarrow} = 0$ in the interior). However, the concentration in the boundary layer is smaller in the case with LC present, since the boundary layer deepens more rapidly due to more efficient entrainment (but also partly because the integration time for the LC case is of somewhat shorter duration). [12] The $\kappa_{v,0\rightarrow}(z)$ profiles in Fig. 6(c) again show the convex shape of $G(\sigma)$. Their values are slightly larger than for density, by about 30%. Again the case with LC shows enhanced mixing, here by a factor $\mathscr{E} = 3.33$. Thus, to within appropriately modest expectations for the accuracy of a parameterization scheme, the form-boundary mixing is also well fit by the proposed KPP generalization.

A to-boundary scalar field, $c_{\rightarrow 0}$, has no surface flux and an initial distribution that is a constant in the interior (i.e., where the density field is initially stably stratified) and zero in the boundary layer region. With time its boundary layer concentration increases, due to the entrainment flux as the boundary layer deepens. Figure 7 shows the mean, turbulent-flux, and eddy-diffusivity profiles for $c_{\rightarrow 0}$ during the slowly evolving, quasi-equilibrium phase. In this case, the non-gradient flux is zero since $F_{\rightarrow 0} = 0$, hence the calculation of $\kappa(z)$ from (5) is by the traditional flux/gradient relation. In Fig. 7(a) there is a greater mean concentration of $c_{\rightarrow 0}$ in the boundary layer in Langmuir turbulence than in shear turbulence due to the enhanced entrainment flux by LC (Fig. 7(b)). The resulting diffusivity, $\kappa_{\rightarrow 0}$, is again convex in shape and larger in magnitude for Langmuir turbulence. The diffusivity is larger for a to-boundary scalar than for a from-boundary scalar, only slightly so in shear turbulence but more so in Langmuir turbulence (i.e., $\kappa_{\rightarrow 0}/\kappa_{0\rightarrow} \approx 1.2$ for the peak magnitudes), but to a lesser degree than has been diagnosed for free convection. [13] The enhancement

[12] We are not concerned about this modest inconsistency in the averaging times because the mean gradient and turbulent flux, and thus the $\kappa_v$, are all rather insensitive to the mean concentration except near the interior edge of the boundary layer.

[13] But there is also LES evidence that this diffusivity ratio in free convection has a dependence on the interior stratification (Sorbjan, 1996).

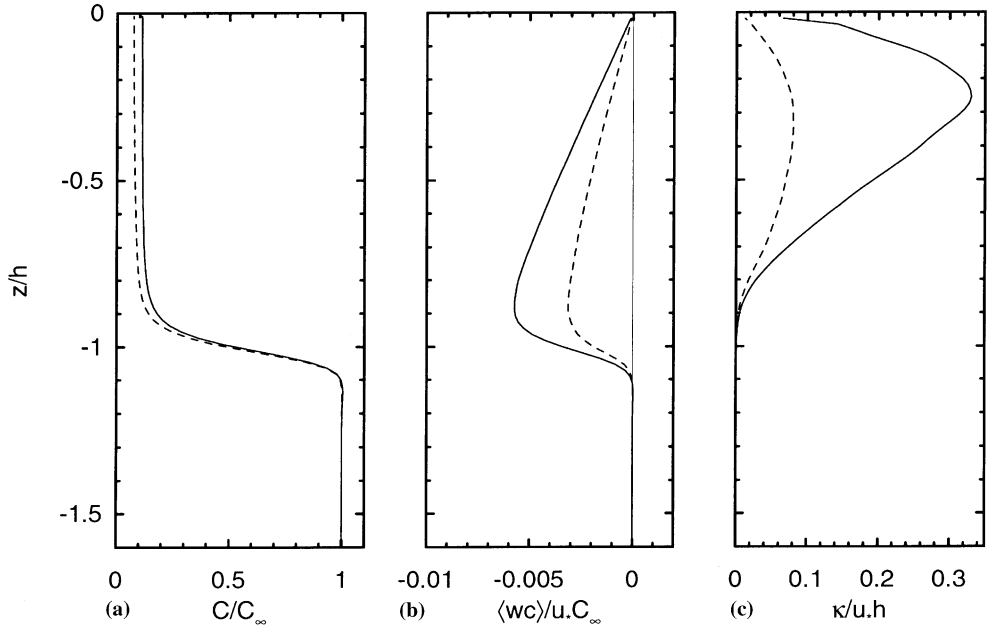


**Fig. 7** Vertical profiles related to the to-boundary scalar concentration, $c_{\rightarrow 0}$, for LES cases with and without LC effects (i.e., $La = 0.3$ [solid] and $\infty$ [dashed]): (a) mean, $\langle c_{\rightarrow 0}\rangle(z)$ (normalized by $c_* = \langle c_{\rightarrow 0}\rangle(-60\text{ m})$); (b) turbulent flux, $\langle c'_{\rightarrow 0}\omega'\rangle(z)$ (normalized by $c_* u_*$); and (c) eddy diffusivity, $\kappa_{v,\rightarrow 0}(z)$ (normalized by $u_* h$).

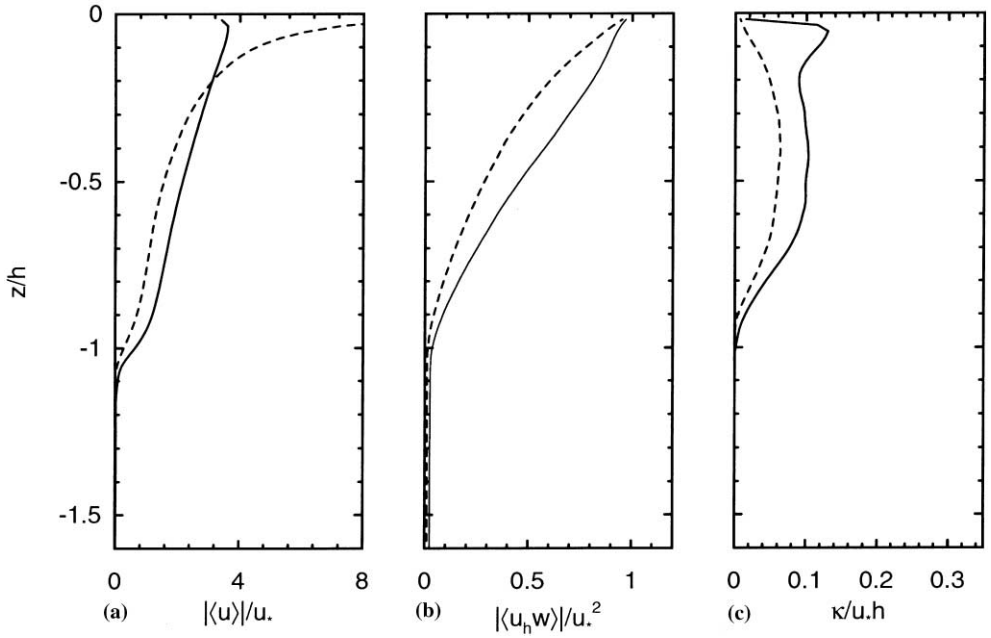


**Fig. 8** Vertical profiles related to the horizontal velocity, $\mathbf{u}_h$, for LES cases with and without LC effects (i.e., $La = 0.3$ [solid] and $\infty$ [dashed]): (a) mean, $|\langle \mathbf{u}_h\rangle(z)|$ (normalized by $u_*$); (b) turbulent flux, $|\langle \mathbf{u}'_h w'\rangle|(z)$ (normalized by $u_*^2$); and (c) eddy diffusivity, $\kappa_{v,\mathbf{u}_h}(z)$ (normalized by $u_* h$), assuming $\mathscr{C}_\gamma = 0$ in (13).

factor for the peak values of $\kappa_{\rightarrow 0}$ is $\mathscr{C} \approx 4.1$, somewhat larger than for $\rho$ and $c_{0\rightarrow}$. Thus, the incompleteness of the present KPP rules (by not distinguishing diffusivities for to- and from-boundary scalars) is still demonstrable for Langmuir turbulence, albeit to a much lesser degree than for free convection. In any event, modeling errors in to-boundary mixing are less onerous than in from-boundary mixing for spilled, buoyant pollutants that are being carried downward from the surface.

Finally, we examine the momentum mixing effects of LC. Although $\mathbf{u}_h$ is a vector quantity, we contract our analysis in Fig. 8 to scalar profiles of the magnitude of the mean current and turbulent momentum

flux, and we evaluate a scalar eddy diffusivity by multiplying the KPP vector momentum flux relation (cf., eqn (5)),

$$F_{\mathbf{u}_h}(z) = \kappa_{v,\mathbf{u}_h}(z)\left[\frac{\partial\langle\mathbf{u}_h\rangle}{\partial z} + \mathscr{C}_\gamma \frac{u_*^2}{Wh}\hat{\mathbf{x}}\right] \tag{13}$$

by the vector mean shear, $\partial\langle\mathbf{u}_h\rangle/\partial z$, to obtain a mean dissipation rate profile. Here $\kappa_{v,\mathbf{u}_h}$ again is assumed to have the KPP form (7), and the obvious vector interpretation has been made for (10) and (12). The mean current has a weaker shear and the turbulent fluxes are larger when LC are present (Figs. 8(a,b)), [14] and the corresponding eddy diffusivity (Fig. 8(c)) is larger with LC, as it is for the material concentrations (Figs. 4, 6, & 7). [15]

Present KPP rules say that $\mathscr{C}_\gamma^* = \mathscr{C}_\gamma = 0$ for momentum (Section 3), and this choice is used in Fig. 8(c). For the case without LC (i.e., $La = \infty$), the shape of $\kappa(z)$ has the convex shape of $G(\sigma)$ in KPP, and the peak magnitude again closely matches the KPP formula, viz., $\kappa/u_*h = k/\phi \cdot \max[G] \approx 0.063$ in (7). However, $\kappa(z)$ for the case with LC (i.e., $La = 0.3$) departs from the convex shape by having an extra, shallow maximum at $z/h \approx -0.05$ where the mean shear is very weak (Fig. 8(a)) while the momentum flux is not weak (Fig. 8(b)), and the degree of enhancement (i.e., the factor $\mathscr{E}$ in (11)) is smaller in the lower part of the boundary layer than we have seen for the material concentrations. Thus, the simple generalization of KPP proposed above, while qualitatively apt (hence better than it would be without the LC modifications), is not highly accurate for momentum flux: perhaps on average in $z$ there is an enhancement of the magnitude of $\kappa$ by a factor $\mathscr{E} \approx 3$ (close to what occurs for the material concentrations), but the shape of $\kappa$, hence also the shape of a $\langle\mathbf{u}_h\rangle(z)$ that would be calculated with this generalized KPP model, are not correct by the standard of the LES solution.

We believe that the present LES and KPP formulations (Sections 2–3) are deficient in their representation of surface gravity wave effects by the absence of enhanced dissipation near the surface – and probably also the turbulent flux of at least momentum – caused by surface wave breaking (e.g., see Terray *et al.*, 1996). One could therefore argue that the seemingly anomalous $\kappa(z)$ structure in Fig. 8(c) should not be taken too seriously until this deficiency is remedied. Nevertheless, we now offer, in a highly speculative way, a couple of possible further modifications of the KPP rules that can recover, to some degree, the expected convex shape and magnitude enhancement of $\kappa$ in the presence of LC.

The first alternative modification is to allow $\mathscr{C}_\gamma \neq 0$ in (13) when $La$ is finite. We choose the value of $\mathscr{C}_\gamma$ to bring the shape of $\kappa(z)$ as close as possible to the convex function $G(\sigma)$ in (8); for $\mathscr{C}_\gamma = 6.9$, the result is shown in Fig. 9(a), which indeed is rather close to the $\kappa(z)$ profiles for the material concentrations in Figs. 4, 6, & 7. The disadvantage of this modification of the KPP rules is that it implies an added parametric complexity for the model: [1] this value of $\mathscr{C}_\gamma$ for momentum is rather different from that for the material properties, $\rho$ and $c_{0\rightarrow}$ (i.e., $\mathscr{C}_\gamma \approx 1.04$) and [2] we cannot apply the same value of $\mathscr{C}_\gamma$ to the shear case without excessively distorting its $\kappa(z)$ profile from the expected convex shape (although using the smaller material-concentration value for $\mathscr{C}_\gamma$ would make little difference in the dashed line in Fig. 9(a)).

The second alternative modification is to change the KPP momentum-flux from (13) to the following form involving the shear in the Stokes drift:

$$F_{\mathbf{u}_h}(z) = \kappa_{v,\mathbf{u}_h}(z)\left[\frac{\partial\langle\mathbf{u}_h\rangle}{\partial z} + \frac{\partial u^s}{\partial z}\right]. \tag{14}$$

This form has the advantage that no modification of the present KPP rules is implied except in the regime of Langmuir turbulence where $\mathbf{u}^s \neq 0$. The primary rationale for this form is that it makes the term involving turbulent momentum flux into a sign-definite production of turbulent kinetic energy; i.e.,

$$\begin{aligned}\frac{\partial e}{\partial t} + \cdots &= -\langle\mathbf{u}_h' w'\rangle \cdot \left(\frac{\partial\mathbf{u}_h}{\partial z} + \frac{\partial\mathbf{u}^s}{\partial z}\right) \\ &= \kappa_{v,\mathbf{u}_h}(z)\left(\frac{\partial\langle\mathbf{u}_h\rangle}{\partial z} + \frac{\partial u^s}{\partial z}\right)^2 \geqslant 0\end{aligned} \tag{15}$$

for any $\kappa_{v,\mathbf{u}_h} \geqslant 0$ (see eqn (5.1) in McWilliams *et al.*, 1997), whereas other forms are ambiguous in their energetic implications a priori. The result of fitting this form – by vector multiplication of (14) with the sum of the mean velocity and Stokes shears – is shown in Fig. 9(b). The $\kappa(z)$ profile again has a convex shape, although its peak amplitude occurs somewhat deeper (near $z/h = -0.5$) than with $G(\sigma)$, and its enhancement factor is closer to $\mathscr{E} \approx 2$ than the values $\mathscr{E} \approx 3$–4 found for the material concentrations.

## Conclusions

In this paper we analyze LES cases with surface-wave-averaged dynamical equations and show that the

[14] See McWilliams *et al.* (1997) for a more extensive interpretation of how LC modify the Ekman currents.

[15] In preparing this manuscript we discovered that we previously made an error in calculating $\kappa(z)$ for the case with LC shown in Fig. 3(c) of McWilliams *et al.* (1997). The present Fig. 8(c) corrects this error. We intend to publish an erratum after further research on the momentum mixing issues that are broached here somewhat speculatively.

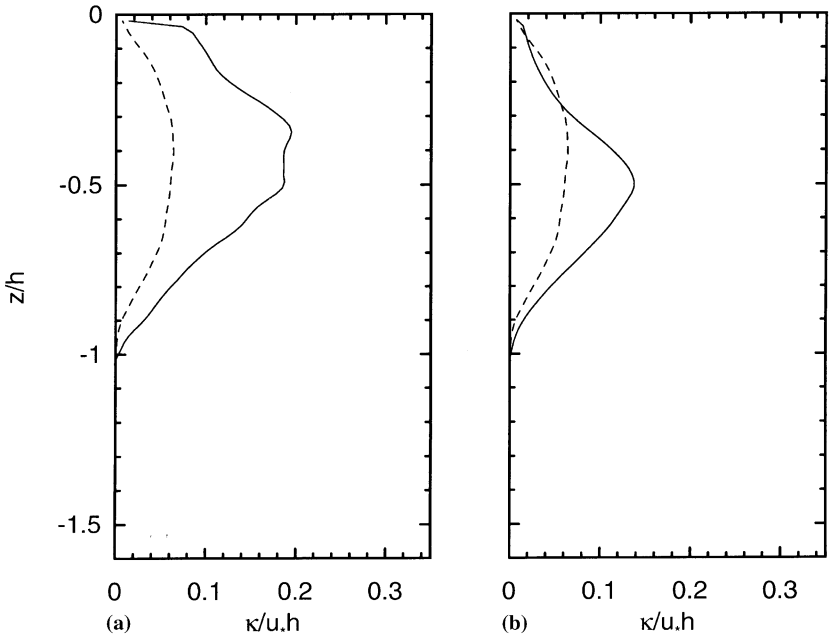


**Fig. 9** Modified eddy diffusivities for horizontal velocity, $\kappa_{v,\mathbf{u}_h}(z)$ (normalized by $u_* h$), for LES cases with and without LC effects (i.e., $La = 0.3$ [solid] and $\infty$ [dashed]): (a) with a non-gradient flux in (13) but only for the case with $La = 0.3$ (with $\mathscr{C}_\gamma = 6.9$); (b) with the alternative flux relation (14).

effect of LC is to make the vertical mixing substantially more efficient for both material properties and momentum. We provide a new confirmation that the previously proposed KPP model accurately characterizes the turbulent transport in a weakly convective, wind-driven boundary layer with stable interior stratification. We also propose a modest generalization of KPP for the regime of weakly convective Langmuir turbulence with two changes to its rules: [1] an increasing value for the turbulent velocity scale, $W$, in (11) for decreasing Langmuir number $La(=\sqrt{u_*/U^s})$ such that $W \sim U^s$ for $La \ll 1$ (as observed and as calculated in LES cases) and [2] a decreasing value of the non-gradient flux coefficient, $\mathscr{C}_\gamma$ as $h/Z < 0$ increases from its large negative value in strong convection. These modifications make the KPP turbulent flux profiles match reasonably well those in the LES case with LC present, especially so for material properties, and even more especially so for density and from-boundary scalars. However, there remain open issues about how well the present LES and KPP formulations represent the momentum flux in Langmuir turbulence, in part because wave-breaking effects are not yet included, and we speculate on several alternative KPP formulations for the momentum flux.

Because of its mathematical simplicity (hence computational efficiency) and its modest initialization and forcing requirements (i.e., a locally measured vertical profile of $T$, $S$, and $\mathbf{u}_h$ plus a meteorological estimate of the surface stress and buoyancy flux), the KPP model is potentially a useful tool for assessing and predicting the movement of spilled material in the ocean and guiding actions undertaken for its amelioration. We believe this paper demonstrates the potential accuracy of KPP for vertical mixing, although many additional steps are needed before it could be applied in practice. The latter include further testing of the KPP predictions; exploring further the dependences on $La, h/Z$, and $h/\lambda$; including the particular rheological and buoyancy properties of oil or other spilled materials; and creating an operationally practical implementation of the observational and modeling system.

***Acknowledgements***—We thank Debra Simchek-Beatty and William Lear (NOAA Hazardous Materials Office) for organizing a conference on the effects of Langmuir circulations and transport of hazardous buoyant materials (oil spills). We appreciate research support by the National Science Foundation through NCAR and by the Office of Naval Research (grants N00014-92-F-0117 and N00014-98-1-0165).

## *References*

Ayotte, K.W., Sullivan, P.P., Andren, A., Doney, S.C., Holtslag, A., Large, W.G., McWilliams, J.C., Moeng, C.-H., Otte, M., Tribbia, J., Wyngaard, J.C., 1996. An evaluation of neutral and convective planetary boundary layer parameterizations relative to large eddy simulation. Boundary-Layer Meteorology 79, 131–175.

Craik, A.D.D., Leibovich, S., 1976. A rational model for Langmuir circulations. Journal of Fluid Mechanics 73, 401–426.

Deardorff, J.W., 1972. Numerical investigation of neutral and unstable planetary boundary layers. Journal of the Atmospheric Sciences 29, 91–115.

Holtslag, A.A.M., Moeng, C.-H., 1991. Eddy diffusivity and countergradient transport in the convective atmospheric boundary layer. Journal of the Atmospheric Sciences 48, 1690–1698.

Large, W.G., McWilliams, J.C., Doney, S.C., 1995. Oceanic vertical mixing: A review and a model with a nonlocal boundary layer parameterization. Review of Geophysics 32, 363–403.

Large, W.G., Danabasoglu, G., Doney, S.C., McWilliams, J.C., 1997. Sensitivity to surface forcing and boundary layer mixing in a global ocean model: Annual-mean climatology. Journal of Physics Ocean 27, 2418–2447.

Large, W.G., Gent, P.R., 1999. Validation of vertical mixing in an equatorial ocean model using large eddy simulations and observations. Journal of Physics Ocean 29, 449–464.

Leibovich, S., 1983. The form and dynamics of Langmuir circulations. Annual Revision of Fluid Mechanics 15, 391–427.

Li, X., Chao, Y., McWilliams, J.C., Fu, L.-L., 2000. A comparison of two vertical mixing schemes in a pacific ocean general circulation model. Journal of Climate (in press).

McWilliams, J.C., Sullivan, P.P., Moeng, C.H., 1997. Langmuir turbulence in the ocean. Journal of Fluid Mechanics 334, 1–30.

McWilliams, J.C., Moeng, C.-H., Sullivan, P.P., 1999. Turbulent fluxes and coherent structures in marine boundary layers: investigations by large-eddy simulation. In: Geernaert, G. (Ed.), Air–Sea Exchange: Physics, Chemistry, Dynamics, and Statistics, Kluwer, Dordrecht, The Netherlands, pp. 507–538.

McWilliams, J.C., Restrepo, J.M., 1999. The wave-driven ocean circulation. Journal of Physics Ocean 29, 2523–2540.

O'Brien, J.J., 1970. A note on the vertical structure of the eddy exchange coefficient in the planetary boundary layer. Journal of the Atmospheric Sciences 27, 1213–1215.

Plueddemann, A.J., Smith, J.A., Farmer, D.M., Weller, R.A., Crawford, R.A., Pinkel, R., Vagle, S., Gnanadesikan, A., 1996. Structure and variability of Langmuir circulation during the surface wave processes program. Journal of Geophysical Research 101, 3525–3543.

Skyllingstad, E.D., Denbo, D.W., 1995. An ocean large-eddy simulation of Langmuir circulations and convection in the surface mixed layer. Journal of Geophysical Research 100, 8501–8522.

Skyllingstad, E.D., Smyth, W.D., Moum, J.N., Wijesekera, H., 1999. Upper ocean turbulence during a westerly wind burst: a comparison of large-eddy simulation results and microstructure measurements. Journal of Physics Ocean 29, 5–28.

Skyllingstad, E.D., Smyth, W.D., Crawford, G.B., 2000. Resonant wind-driven mixing in the ocean boundary layer. Journal of Physics Ocean 30, 1866–1890.

Skyllingstad, E.D., 2000. Scales of Langmuir circulation generated using a large-eddy simulation model. Spill Science & Technology 6 (3/4), 239–246.

Smith, J.A., 1998. Evolution of Langmuir circulation during a storm. Journal of Geophysical Research 103, 12649–12688.

Smith, J.A., 1999. Observations of wind, waves, and the mixed layer: the scaling of surface motion. In: Banner, M.L. (Ed.), Wind-Driven Air-Sea Interface: Electromagnetic and Acoustic Sensing, Wave Dynamics, and Turbulent Fluxes, University of New South Wales, Sydney, pp. 231–238.

Sorbjan, Z., 1996. Effects caused by varing strength of the capping inversion based on a large-eddy simulation of the shear-free convective boundary layer. Journal of the Atmospheric Sciences 53, 2015–2024.

Terray, E.A., Donelan, M.A., Agrawal, Y.C., Drennan, W.M., Kahma, K.K., III, A.J, Hwang, P.A., Kitaigorodskii, S.A., 1996. Estimates of kinetic energy dissipation under breaking waves. Journal of Physics Ocean 26, 792–807.

Troen, I.B., Mahrt, L., 1986. A simple model of the atmospheric boundary layer: Sensitivity to surface evaporation. Boundary-Layer Meteorology 37, 129–148.

Wyngaard, J.C., Brost, R.A., 1984. Top-down and bottom-up diffusion of a scalar in the convective boundary layer. Journal of the Atmospheric Sciences 41, 102–112.

Wyngaard, J.C., 1987. A physical mechanism for the asymmetry in top-down and bottom-up diffusion. Journal of the Atmospheric Sciences 44, 1083–1087.

Wyngaard, J.C., Weil, J.C., 1991. Transport asymmetry in skewed turbulence. Physics of Fluids A3, 155–162.